



TITLE:

DFT study of CO oxidation over Au/TiO₂(110): The extent of the reactive perimeter zone

AUTHOR(S):

Koga, Hiroaki; Tada, Kohei; Okumura, Mitsutaka

CITATION:

Koga, Hiroaki ...[et al]. DFT study of CO oxidation over Au/TiO₂(110): The extent of the reactive perimeter zone. Chemical Physics Letters 2014, 610-611: 76-81

ISSUE DATE:

2014-08

URL:

<http://hdl.handle.net/2433/189420>

RIGHT:

© 2014 Elsevier B.V.; This is not the published version. Please cite only the published version.; この論文は出版社版ではありません。引用の際には出版社版をご確認ご利用ください。

DFT study of CO oxidation over Au/TiO₂(110): The extent of the reactive perimeter zone

Hiroaki Koga^{a,*}, Kohei Tada^b, Mitsutaka Okumura^{a,b}

^a Elements Strategy Initiative for Catalysts and Batteries (ESICB), Kyoto University, 1-30 Goryoohara, Kyoto 615-8245, Japan

^b Department of Chemistry, Graduate School of Science, Osaka University, 1-1 Machikaneyama, Toyonaka, Osaka 560-0043, Japan

*Corresponding author. E-mail: koga.hiroaki.6u@kyoto-u.ac.jp, phone: +81-75-383-3043, fax: +81-75-383-3047.

Keywords

Au catalyst, rutile TiO₂, O₂ adsorption, CO oxidation, DFT

Abstract

O₂ adsorption and CO oxidation on a Au/rutile TiO₂(110) catalyst have been examined by DFT in order to define the extent of the reactive perimeter zone. O₂ is found to adsorb on the five-fold coordinated Ti sites that are away from the perimeter as well as on those next to the perimeter. Both O₂ show similar reactivity toward a gaseous CO. CO oxidation still occurs predominantly at the perimeter because O₂ adsorption is strongest at the perimeter Ti site and because CO is activated on Au through back donation.

1. Introduction

Gold was traditionally regarded as the unlikeliest candidate for oxidation catalysts because of its inability to adsorb and dissociate oxygen. This view has changed drastically since gold nanoparticles (NP) supported on oxides such as TiO_2 were discovered to exhibit extraordinary catalytic activity for low-temperature CO oxidation [1,2] and other useful reactions [3]. Numerous experimental and theoretical efforts have been made to find the origin of catalytic activity of gold catalysts [3], especially the location of active sites. It is generally viewed that CO oxidation occurs along the perimeter of Au/oxide interface ('perimeter hypothesis') [4]. For the most basic case of Au/ TiO_2 , this hypothesis has recently been confirmed by experiments showing the proportionality between the rate of oxidation and the length of perimeter [5,6].

However, it is still unclear whether the reactive zone is confined to the immediate vicinity of the perimeter or includes the nearby TiO_2 surface. The exact determination of the active sites requires quantum-chemical approaches such as the density-functional theory (DFT) [7,8]. Earlier DFT calculations have found that, although the stoichiometric rutile $\text{TiO}_2(110)$ surface is unable to adsorb O_2 in the absence of Au NPs [9], the five-fold coordinated Ti (Ti^{5c}) sites next to the perimeter are able to adsorb and activate O_2 [9-12]. This is because the Ti cation lowers the antibonding π orbital of O_2 below the Au Fermi level, enabling electron transfer from the Au to O_2 , and binds with the resulting O_2 anion [9,10]. Because the ability to lower O_2 π^* is innate to TiO_2 [10], Ti^{5c} sites away from the perimeter may also be able to adsorb and activate O_2 .

In this study, therefore, O_2 adsorption and CO oxidation on a Au/rutile $\text{TiO}_2(110)$ catalyst are examined by DFT in order to determine the extent of the reactive perimeter zone. The remainder of this letter is organized as follows. Section 2 describes the details of calculation. Section 3.1 examines O_2 adsorption and shows that O_2 is strongly adsorbed and activated on Ti^{5c} sites both next to and away from the perimeter. Section 3.2 examines CO oxidation and shows that these O_2 are almost equally reactive toward a gaseous CO, but that the energy barrier is smaller at the perimeter where O_2 can react with CO on Au. It is concluded in Section 4 that the reactive zone is confined to the immediate vicinity of the perimeter because O_2 adsorption is strongest at the perimeter Ti^{5c} site and because CO is activated on Au.

2. Method

Total energies and optimized geometries were calculated by a plane-wave DFT code STATE (Simulation Tool for Atom TEchnology) [13]. This code has been applied to various systems including Au(111) and Au/TiO₂ [14-16]. The exchange-correlation functional by Perdew, Burke, and Ernzerhof was employed [17]. The cutoff energies were 25 and 225 Ry for the Kohn-Sham orbitals and charge density, respectively. The interactions between ionic cores and valence electrons were described by ultrasoft pseudopotentials [18], with 4, 6, 10, and 11 electrons taken as valence for C, O, Ti, and Au, respectively. Spin-unpolarized calculations were performed unless otherwise noted. Transition states (TS) were searched by the force inversion method [19], and then the initial (IS) and final (FS) states were found by relaxation from positions slightly displaced from TS. Charge analysis was done by the Bader method [20] as implemented by Henkelman et al. [21]. The Bader charge is the charge inside a volume defined by the surface on which the normal derivative of the electron density vanishes. The Bader charge does not necessarily match the formal charge state, for example, the Bader charge of O in bulk rutile is calculated to be $-1.1e$. Orbitals were visualized using VESTA (Visualization for Electronic and STructural Analysis) [22].

Fig. 1 shows the model of a Au/TiO₂(110) catalyst used in the calculations. The TiO₂ surface was represented by a periodic slab consisting of four rutile (110) trilayers. The top three trilayers were allowed to move while the bottom one was frozen during geometrical optimization. The periodic images of the slab were separated by 1.39 nm of vacuum. The stoichiometric surface was examined because oxygen vacancies would be readily repaired under oxygen-rich conditions typical with CO oxidation. The perimeter of a Au/TiO₂ catalyst was modeled by placing a Au rod on the rutile surface with the orientation of Au(111)[110]//TiO₂(110)[001]. This is the orientation found by TEM experiments, and the calculated distance between the Au NP and the Ti layer (0.34 nm) is consistent with the measured one (0.33 nm) [23]. The rod consists of three Au(111) layers, the top layer being two-atom wide and the bottom two layers three-atom wide. The Au atoms at the rim of the rod are in register with the bridging O. This model is the same as that used by Green et al. [12], but Au atoms were now allowed to move in three dimensions. Ti^{5c} sites are distinguished by the order of proximity to the perimeter, such

as first, second, and third nearest sites (Fig. 1). Large 4×3 and 6×3 cells, sampled with a 1×2 k-point mesh, were used, where the first and second dimensions refer to $\text{TiO}_2[\bar{1}10]$ and $[001]$.

The stability of an adsorption geometry is expressed in terms of adsorption energy E_{ad} , defined as the total energy of the adsorption geometry minus the total energy of $\text{Au}/\text{TiO}_2(110)$ minus the total energy of gaseous O_2 and/or CO . Here, a gaseous molecule was calculated using a $24\times 24\times 24$ Bohr³ cell (O_2 calculated with spin polarization). According to the above definition, the lower the adsorption energy, the more stable the adsorbate. The energy barrier of reaction was calculated as the total energy of the transition state minus the total energy of the initial state. For a reaction with a gaseous CO , the total energy of the initial state was calculated as the sum of the total energies of the O_2 -adsorbed geometry and a gaseous CO .

Because periodic boundary conditions are used, interactions with the periodic images of the Au rod might result in the overestimation of O_2 adsorption energies. To examine this, we have performed several test calculations for O_2 adsorbed side-on to the nearest Ti^{5c} site (see Section 3.1), varying the width of the cell. The adsorption energy, bond length, and Bader charge on O_2 are reported in Table 1. As can be seen here, the results are practically the same for 3×3 and wider cells, and the error is not very large even at 2×3 . In addition, dependence on k-point mesh and slab thickness (examined using the 2×3 cell) is also small (Table 1).

3. Results and discussion

3.1 O_2 adsorption

We begin with confirming that O_2 cannot be adsorbed on the stoichiometric TiO_2 surface in the absence of the rod, using the 4×3 cell. Fig. 2a shows the equilibrium position for O_2 placed above the Ti^{5c} site. Negligible adsorption energy (-0.04 eV) is obtained for this O_2 . The O_2 bond length is practically unchanged from that (125.4 pm) in the gas phase. O_2 remains in the triplet state, with no charge transferred from the surface. These results are reasonable because, although the Ti cation may be able to lower O_2 π^* , the transfer from the valence band of TiO_2 can only result in overall destabilization. Thus, without the Au rod, the stoichiometric surface is practically

unable to adsorb and activate O₂.

Next, we examine O₂ adsorption at the perimeter of the Au/TiO₂ interface, using the 4×3 cell. First, weak adsorption energy (−0.22 eV) is obtained for O₂ bridging two Au sites at the perimeter (Fig. 2b). Small negative charge and residual spin on O₂ indicate insufficient activation of O₂. In contrast, much stronger adsorption energy (−1.03 eV) is obtained for O₂ bridging Ti^{5c} and Au at the perimeter (Fig. 2c), reproducing an earlier result (−1.01 eV) [12]. The longer O-O bond and negative charge on O₂ indicate that this O₂ is activated to a superoxide state [9]. Most of the charge (−0.51e) is on the lower O, drawn to the Ti cation. Even stronger adsorption energy (−1.74 eV) is obtained for O₂ adsorbed side-on to the Ti^{5c} site next to the perimeter (Fig. 2d). Both O of the O₂ are now bonded to the Ti cation, enhancing the adsorption energy. Even longer O-O bond and more negative charge indicate that this O₂ is activated to a peroxide state [9]. (Negligible spin polarization was found for the superoxide and peroxide states.) In the following, we focus on the side-on O₂ because this is the more stable and further activated species.

We now examine how the O₂ adsorption energy changes with distance from the perimeter, using the 6×3 cell. Figs. 2e-2g show O₂ adsorbed side-on to the Ti^{5c} site that is first, second, and third nearest to the perimeter, respectively. The adsorption is strongest at the first site (−1.70 eV), but the second (−1.43 eV) and third (−1.39 eV) sites are not much higher in energy. Moreover, similar O₂ bond lengths and Bader charges are found for the three sites. Thus, Ti^{5c} sites away from the perimeter also have the ability to adsorb and activate O₂, and this ability appears to weaken very slowly beyond the second nearest site. (There should still be a limit to O₂ adsorption on remote sites because the probability of electron transfer will decrease with distance.)

To explain the above results, we have calculated projected density of states (PDOS) for the Au/TiO₂ surface before O₂ adsorption and the geometries of Figs. 2e-2g. Before O₂ adsorption, the PDOS of the three Ti^{5c} sites are nearly indistinguishable (Fig. 3a). The Fermi level is located slightly below the empty 3d states of Ti^{5c}, indicating that the HOMO of the Au rod is close to the conduction band of TiO₂. This could also imply a small amount of electron transfer to TiO₂, but the amount would not be so large as to

cause significant model-size dependence (see Table 1) or artificial dipole interaction across the vacuum layer (dipole correction [24] for Au/TiO₂ in a 2×1 cell shows that its stability is overestimated by a mere 4 meV).

Fig. 3b shows PDOS for O₂ adsorption on the nearest Ti^{5c} site. The O 2p levels of O₂ appear below the Fermi level, indicating electron transfer from the Au rod to O₂. The peak around −1.7 eV is from O 2p_z and is identified as out-of-plane O₂ π*. The peak around −0.4 eV is from O 2p_x and 2p_y and is identified as in-plane O₂ π*. These states are strongly mixed with the 3d orbitals of Ti^{5c}, confirming that the Ti cation stabilizes O₂ π* [10]. Moreover, the lower peak also coincides with that of the three-fold coordinated O (O^{3c}) immediately below O₂, indicating that this O₂ π* is stabilized so much as to come close to the valence band of TiO₂. This is reasonable considering that they are both Ti-stabilized O 2p states. Because Au HOMO is close to the TiO₂ conduction band while at least one of O₂ π* is brought close to the TiO₂ valence band, electrons are transferred from Au to O₂ through the TiO₂ conduction band. O₂ thus becomes anionic and is bound strongly to the Ti cation. Au states, on the other hand, do not appear to mix strongly with O₂ π*, in fact, Au PDOS is mostly unchanged from that before O₂ adsorption (Fig. 3a).

PDOS for O₂ adsorption on the second and third nearest Ti^{5c} sites (Figs. 3c and 3d, respectively) are similar to that for the nearest site (Fig. 3b). Again, strong interaction with the Ti cation lowers the O 2p levels of O₂ below the Fermi level, causing electron transfer from the Au rod to O₂. The out-of-plane O₂ π* also mixes with O^{3c} p_z. The only difference is a small shift of O₂ π* peaks to lower energy when O₂ is next to the perimeter (Fig. 3b). This is not caused by orbital interaction with Au because Au PDOS is almost identical in Figs. 3b-3d. Moreover, there appears to be little difference between the PDOS of the three Ti^{5c} sites before O₂ adsorption (Fig. 3a). Hence the shift is attributed to the influence of the positive charge left on the Au rod after electron transfer to O₂.

In summary, we have confirmed strong adsorption of O₂ to the Ti^{5c} site of TiO₂ in the presence of the Au rod. The adsorption is strong also at Ti^{5c} sites away from the perimeter. This is because the Ti cation is chiefly responsible for stabilizing O₂ π*. The

Au rod plays an essential but passive role of electron reservoir, raising the Fermi level so that $O_2 \pi^*$ is filled. Still, the adsorption is strongest at the perimeter Ti^{5c} site because the positive charge left on the rod provides additional stabilization to the O_2 anion.

3.2 CO oxidation

Because O_2 molecules are activated to a similar extent whether they are on the first or second nearest Ti^{5c} sites, we expect them to react similarly to a gaseous CO. On the other hand, O_2 on the nearest site can also react with CO adsorbed on the rim of the Au rod (Au-CO). We thus examine three cases of CO oxidation: (i) the nearest O_2 reacting with Au-CO (Figs. 4a-4c), (ii) the nearest O_2 reacting with a gaseous CO (Figs. 4d-4f), and (iii) the second nearest O_2 reacting with a gaseous CO (Figs. 4g-4i). The results presented in this section were obtained using the 4×3 cell.

For the reaction of Au-CO with the nearest O_2 , we find the initial and transition states shown in Figs. 4a and 4b, respectively. A search for the final state resulted in CO_2 desorption as shown in Fig. 4c, so CO_2 desorbs spontaneously after reaction. The energy barrier is calculated to be 0.22 eV, consistent with the low-temperature catalytic activity of Au/ TiO_2 . In the initial state (Fig. 4a), CO is adsorbed head-on to the perimeter Au site. The Au-O^{br} bond there is broken as a result. The plot of a Kohn-Sham orbital directly below the Fermi level shows the hybridization between Au states and an antibonding π orbital of CO, indicating back donation from the Au rod to CO (Fig. 5). On the other hand, the state of O_2 activation is unaffected by CO adsorption: The O_2 bond length and the charge on O_2 are similar to those before CO adsorption (Table 2). In proceeding from the initial to transition state, the distance between O_2 and CO is greatly decreased, whereas neither the O_2 bond length nor the charge on O_2 is changed much (Table 2). That is, the transition state is reached without further activation of O_2 . The energy barrier is thus mostly due to the exchange repulsion between O_2 and CO, and not due to the cost of breaking the O_2 bond.

For the reaction of a gaseous CO with the nearest O_2 , we find the transition state shown in Fig. 4e. Relaxation from this transition state resulted in desorption of CO and CO_2 as shown in Figs. 4d and 4f, respectively, so a gaseous CO reacts directly with the O_2 anion to produce a gaseous CO_2 . The calculated energy barrier (0.56 eV) is small, but

not as small as that (0.22 eV) for the reaction with Au-CO. Because the gaseous CO reacts directly with O₂, the reaction depends heavily on O₂ activation, requiring more activation energy. In fact, the O-O bond is stretched further and O₂ is made more negative at the transition state (Table 2).

The reaction of a gaseous CO with the second nearest O₂ is very much similar to that with the nearest O₂. The calculated transition state is shown in Fig. 4h. Relaxation from this transition state resulted in desorption of CO and CO₂ as shown in Figs. 4g and 4i, respectively, so a gaseous CO reacts directly with the O₂ anion to produce a gaseous CO₂. The calculated energy barrier (0.57 eV) is almost equal to that for the nearest O₂ (0.56 eV). The stretching of the O-O bond and the more negative charge on O₂ at the transition state indicate that the reaction requires further activation of O₂ (Table 2).

4. Conclusions

We have performed DFT calculations for O₂ adsorption and CO oxidation on the rutile TiO₂(110) surface supporting a Au rod. First, we have confirmed that O₂ is strongly adsorbed and activated on the Ti^{5c} site next to the perimeter ($E_{\text{ad}} \sim -1.7$ eV). The large energy generated by adsorption will assist desorption of contaminants from the oxide surface, releasing additional Ti^{5c} sites for O₂ adsorption. Then, we have found strong adsorption energies ($E_{\text{ad}} \sim -1.4$ eV) also for Ti^{5c} sites away from the perimeter. This is because the Ti cation is mostly responsible for O₂ adsorption, by stabilizing O₂ π^* , enabling electron transfer from the Au rod to O₂, and binding the resulting O₂ anion. The role of the Au rod is primarily to donate electrons to O₂ although positive charge left on it provides some additional stabilization to the O₂ anion.

O₂ adsorbed on the second nearest Ti^{5c} site is almost as active as that on the perimeter Ti^{5c} site, in fact, we have found almost identical energy barriers (0.57 and 0.56 eV, respectively) for the reaction with a gaseous CO. At room temperature and below, however, CO oxidation still occurs predominantly at the perimeter for two reasons. First, the adsorption is strongest at the perimeter because of the influence of the positive charge of the Au rod on the O₂ anion. Even the small energy difference (~ 0.3 eV) translates to a Boltzmann factor of 10^4 and more at low temperatures. The probability of electron transfer should also decrease with distance from the perimeter. Second, the

barrier is much smaller (0.22 eV) for the reaction between O₂ on the perimeter Ti^{5c} site and CO on the Au rod because CO is activated by back donation from Au. At higher temperatures, on the other hand, O₂ appears to react on the surface of a Au NP [6]. Under such conditions, the Au NP is likely to donate electrons directly to O₂ on its surface, instead of transferring them to O₂ on Ti^{5c} sites. Thus, at least with the conventional TiO₂-supported Au NP catalysts, the catalytic activity of remote Ti^{5c} sites makes comparatively little contributions to the rate of CO oxidation. The remote sites can still be useful when the perimeter sites are poisoned with contaminants, for example.

In conclusion, Ti^{5c} sites away from the perimeter of Au/TiO₂ also have the ability to adsorb and activate O₂. CO oxidation still occurs predominantly along the perimeter because O₂ adsorption is strongest at the perimeter Ti^{5c} site and because CO is activated on Au. Thus, the reactive zone is confined to the immediate vicinity of the perimeter.

Acknowledgments

This work was performed under a management of ‘Elements Strategy Initiative for Catalysts and Batteries (ESICB)’ supported by Ministry of Education, Culture, Sports, Science and Technology, Japan (MEXT).

References

- [1] M. Haruta, N. Yamada, T. Kobayashi, S. Iijima, *J. Catal.* 115 (1989) 301.
- [2] M. Okumura, S. Nakamura, S. Tsubota, T. Nakamura, M. Azuma, M. Haruta, *Catal. Lett.* 51 (1998) 53.
- [3] T. Takei, T. Akita, I. Nakamura, T. Fujitani, M. Okumura, K. Okazaki, J.H. Huang, T. Ishida, M. Haruta, *Adv. Catal.* 55 (2012) 1.
- [4] M. Haruta, *Catal. Today* 36 (1997) 153.
- [5] M. Kotobuki, R. Leppelt, D.A. Hansgen, D. Widmann, R.J. Behm, *J. Catal.* 264 (2009) 67.
- [6] T. Fujitani, I. Nakamura, *Angew. Chem. Int. Ed.* 50 (2011) 10144.
- [7] P. Hohenberg, W. Kohn, *Phys. Rev.* 136 (1964) B864.
- [8] W. Kohn, L.J. Sham, *Phys. Rev.* 140 (1965) 1133.
- [9] L.M. Molina, M.D. Rasmussen, B. Hammer, *J. Chem. Phys.* 120 (2004) 7673.
- [10] Z.-P. Liu, X.-Q. Gong, J. Kohanoff, C. Sanchez, P. Hu, *Phys. Rev. Lett.* 91

- (2003) 266102.
- [11] I.N. Remediakis, N. Lopez, J.K. Norskov, *Angew. Chem. Int. Ed.* 44 (2005) 1824.
 - [12] I.X. Green, W. Tang, M. Neurock, J.T. Yates, Jr., *Science* 333 (2011) 736.
 - [13] Y. Morikawa, *Phys. Rev. B* 51 (1995) 14802.
 - [14] K. Okazaki, Y. Morikawa, S. Tanaka, K. Tanaka, M. Kohyama, *Phys. Rev. B* 69 (2004) 235404.
 - [15] K. Okazaki-Maeda, M. Kohyama, *Chem. Phys. Lett.* 492 (2010) 266.
 - [16] K. Tada, K. Sakata, S. Yamada, K. Okazaki, Y. Kitagawa, T. Kawakami, S. Yamanaka, M. Okumura, *Mol. Phys.* 112 (2014) 365.
 - [17] J.P. Perdew, K. Burke, M. Ernzerhof, *Phys. Rev. Lett.* 77 (1996) 3865.
 - [18] D. Vanderbilt, *Phys. Rev. B* 41 (1990) 7892.
 - [19] Y. Tateyama, T. Ogitsu, K. Kusakabe, S. Tsuneyuki, *Phys. Rev. B* 54 (1996) 14994.
 - [20] R. Bader, *Atoms in Molecules: A Quantum Theory*, Oxford University Press, New York, 1990.
 - [21] G. Henkelman, A. Arnaldsson, H. Jonsson, *Comp. Mater. Sci.* 36 (2006) 354.
 - [22] K. Momma, F. Izumi, *J. Appl. Crystallogr.* 44 (2011) 1272.
 - [23] T. Akita, K. Tanaka, M. Kohyama, M. Haruta, *Surf. Interface Anal.* 40 (2008) 1760.
 - [24] J. Neugebauer, M. Scheffler, *Phys. Rev. B* 46 (1992) 16067.

Tables

Table 1. Variation of O₂ adsorption energy E_{ad} , O₂ bond length l , and Bader charge q on O₂ with cell width, k-point mesh, and the number of trilayers L .

Cell	k-mesh	L	E_{ad} (eV)	l (pm)	q (e)
2×3	1×2	6	−1.97	145.8	−0.96
2×3	1×4	4	−1.91	145.9	−0.96
2×3	2×2	4	−1.89	145.7	−0.96
2×3	1×2	4	−1.94	145.7	−0.96
3×3	1×2	4	−1.70	145.7	−0.93
4×3	1×2	4	−1.74	145.5	−0.93
6×3	1×2	4	−1.70	145.5	−0.92

Table 2. Variation of interatomic distance d (pm) and Bader charge q (e) during CO oxidation over Au/TiO₂, calculated using the 4×3 cell. O₂(i): O₂ on the nearest Ti^{5c} site. O₂(ii): O₂ on the second nearest Ti^{5c} site. Au-CO: CO on the Au rod. CO(g): CO from the gas phase.

	$d(\text{O-O})$	$d(\text{C-O})$	$d(\text{O}_2\text{-CO})$	$d(\text{Au-CO})$	$q(\text{O}_2)$	$q(\text{CO})$
O ₂ (i)	145.5				−0.93	
O ₂ (i)+Au-CO IS (Fig. 4a)	145.4	116	262	201	−0.94	+0.03
O ₂ (i)+Au-CO TS (Fig. 4b)	146.0	118	175	207	−0.88	+0.03
O ₂ (i)+CO(g) TS (Fig. 4e)	165.9	117	175		−1.10	+0.11
O ₂ (ii)	145.4				−0.90	
O ₂ (ii)+CO(g) TS (Fig. 4h)	165.4	117	174		−1.07	+0.11

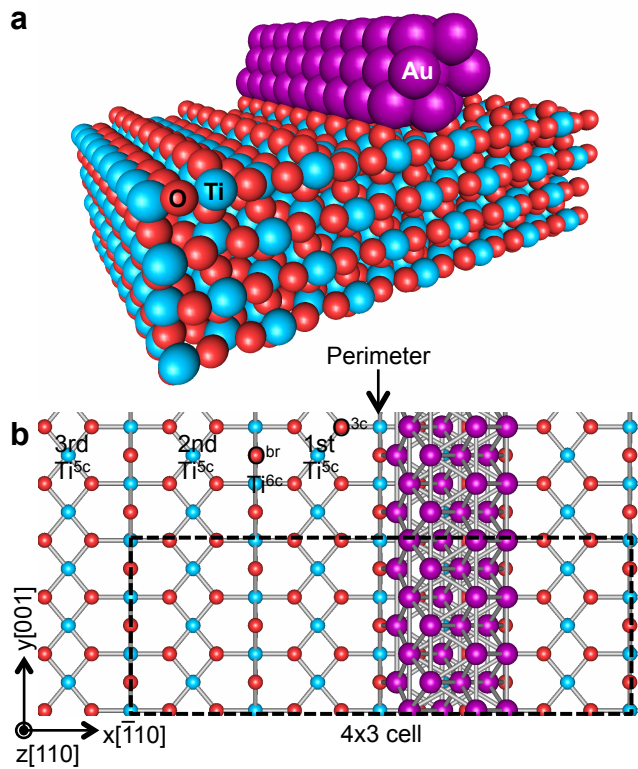


Fig. 1. Perspective (a) and plan (b) views of the Au/TiO₂(110) model. Ti^{5c} , Ti^{6c} , O^{br} , and O^{3c} denote five-fold coordinated Ti, six-fold coordinated Ti, two-fold coordinated bridging O, and three-fold coordinated in-plane O, respectively.

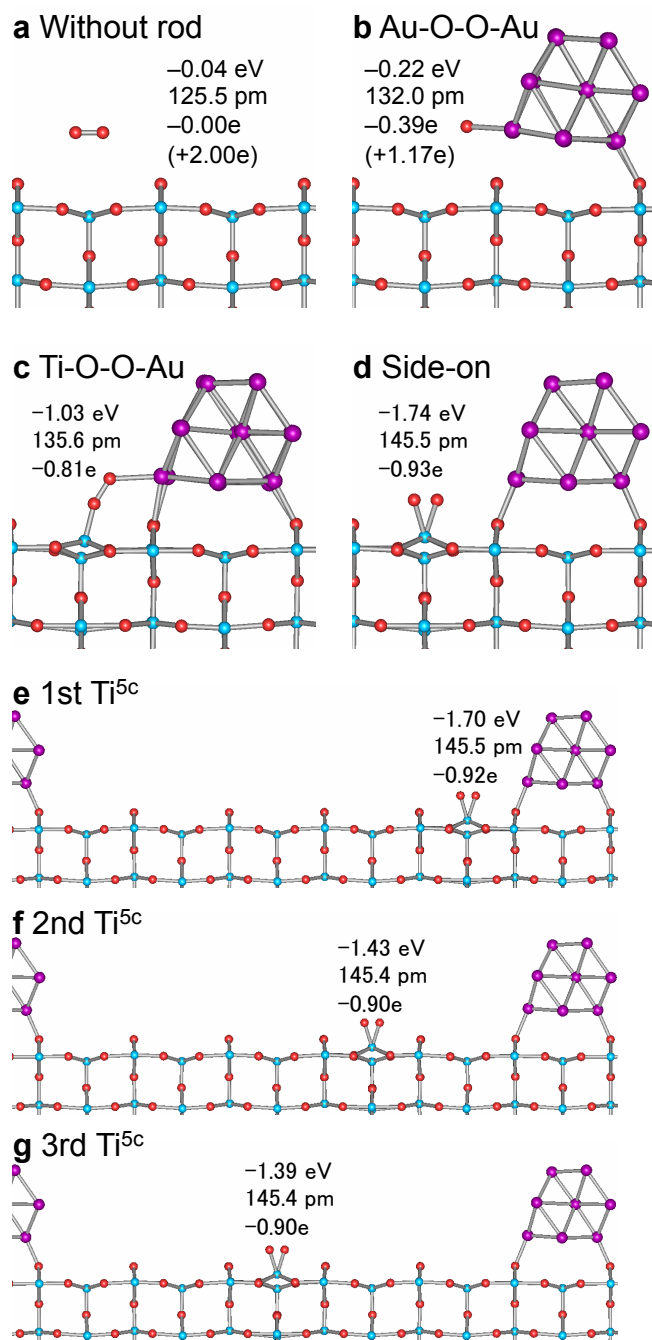


Fig. 2. O_2 on stoichiometric $TiO_2(110)$ (a), O_2 at the perimeter of $Au/TiO_2(110)$ (b-d), and O_2 on Ti^{5c} sites (e-g). (a)-(d) are calculated in 4×3 and (e)-(g) in 6×3 cells. Adsorption energies, O_2 bond lengths, and Bader charges on O_2 (for spin-polarized systems, the difference of up and down Bader charges in parentheses) are displayed in the figure. O_2 in (b) is parallel to the rod axis.

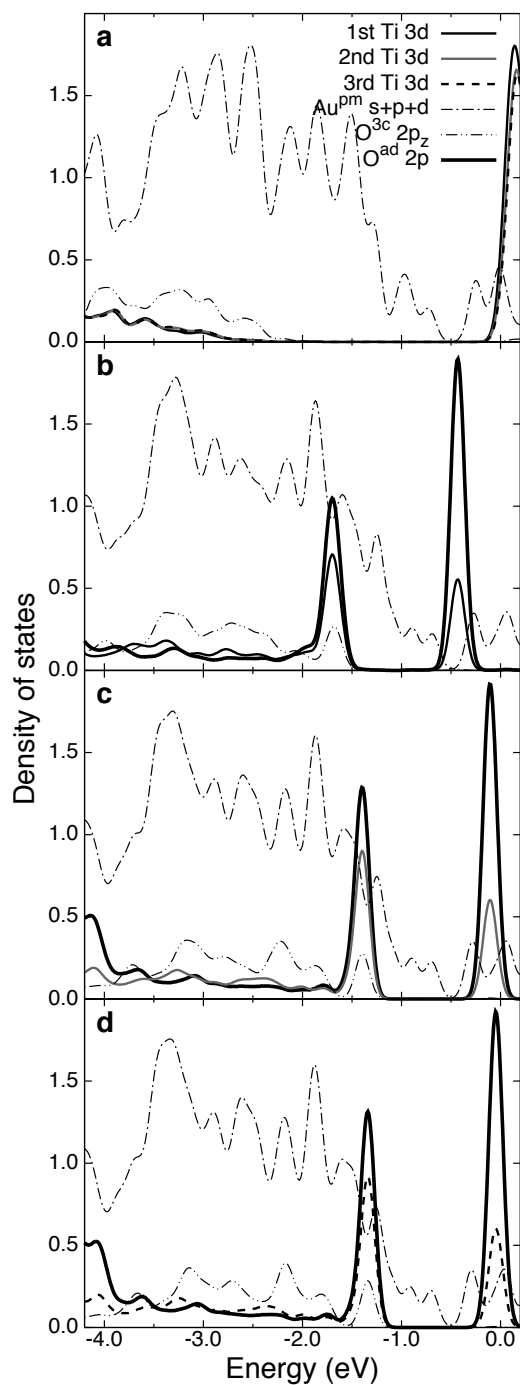


Fig. 3. Projected density of states (PDOS): Before O₂ adsorption (a), O₂ on the first (b), second (c), and third (d) nearest Ti^{5c} sites. Au^{pm} denotes the Au atom at the perimeter of the rod. O^{ad} denotes the O of O₂ that is nearer to the perimeter. O^{3c} denotes the three-fold coordinated in-plane O nearest to the perimeter in (a) and the one directly below O^{ad} in (b)-(d). The Fermi level is at 0 eV. Refer to Fig. 1 for definition of axes. Calculated using the 6×3 cell.

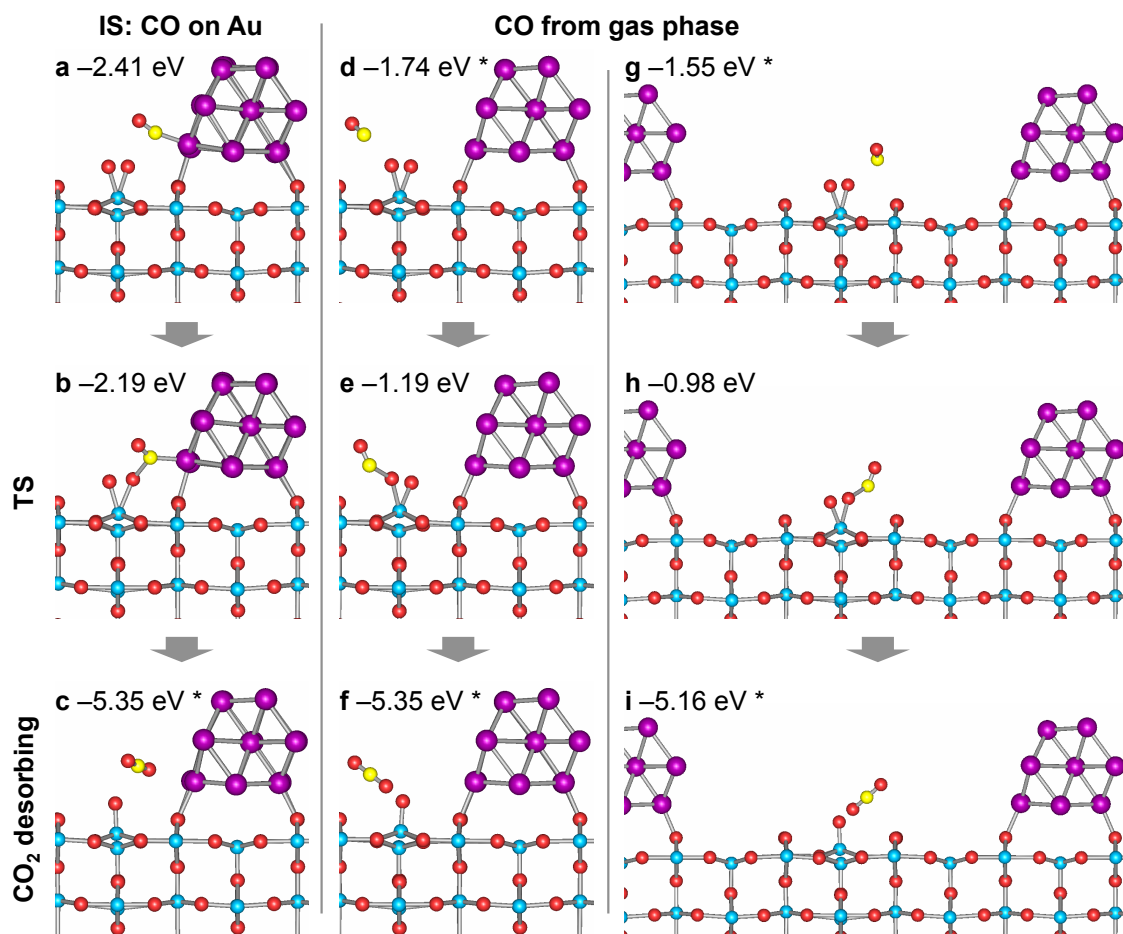


Fig. 4. CO oxidation: O₂ on the nearest Ti^{5c} site reacting with Au-CO (a-c), O₂ on the nearest Ti^{5c} site reacting with a gaseous CO (d-f), and O₂ on the second nearest Ti^{5c} site reacting with a gaseous CO (g-i). Adsorption energies are displayed for IS and TS, and those at the desorption limit for snapshots (marked with an asterisk). Viewed along the rod. Calculated using the 4×3 cell.

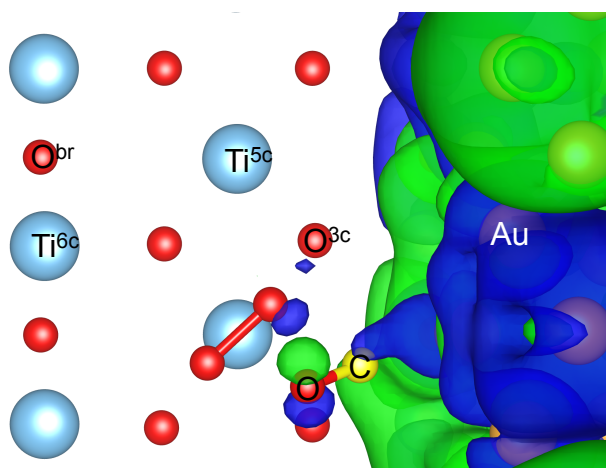


Fig. 5. Highest occupied orbital (at the sampling k point) of the initial state of the reaction between O_2 and Au-CO (isosurface plot of the real part; plan view).